XII International Conference on Computational Plasticity. Fundamentals and Applications
COMPLAS XII
E. Oñate, D.R.J. Owen, D. Peric and B. Suárez (Eds)

FINITE ELEMENT ANALYSES OF FATIGUE CRACK GROWTH UNDER SMALL SCALE YIELDING CONDITIONS MODELLED WITH A CYCLIC COHESIVE ZONE APPROACH

STEPHAN ROTH* AND MEINHARD KUNA*

*TU Bergakademie Freiberg (TUBAF)
Institute of Mechanics and Fluid Dynamics
Lampadiusstraße 4, 09596 Freiberg, Germany
e-mail: Stephan.Roth@imfd.tu-freiberg.de, http://tu-freiberg.de/fakult4/imfd/

Key words: Cyclic Cohesive Zone Model, Fatigue Crack Growth, Boundary Layer, Small Scale Yielding, Damage Mechanics

Abstract. Mode I fatigue crack growth is modelled and investigated with a cohesive zone approach. A 2D finite element boundary layer model under plane strain and small scale yielding conditions is used to generate fatigue crack growth rate curves. This study focuses on the FE model generation with the aim to obtain reliable data of fatigue crack growth rates with computational costs kept as low as possible. In particular, this concerns the choice of geometric quantities of the boundary layer, appropriate mesh sizes and meshing strategies, and the time incrementation. In order to save resource consumption regarding computing time, licenses and memory, the ABAQUS URDFIL interface is used to observe the progress of fatigue crack growth, to control time incrementation and output generation, and to stop the simulation once a stable fatigue crack growth rate is reached. The latter is characterised by a constant amount of dissipated energy per load cycle and steady-state damage and stress profiles in the ligament. Different crack length definitions evaluating both profiles are compared. The resulting fatigue crack growth rate curves including threshold value, static failure load, and Paris region, qualitatively match experimental observations.

1 INTRODUCTION

Tracking cracks under arbitrary loading conditions using finite element (FE) calculations requires a thorough understanding of the specific cracking process and big computational effort especially for cyclic loading. In particular, for interfacial crack growth where the crack path is known, the cohesive zone approach is established. Although there is a large amount of monotonic cohesive zone models documented in the literature (e.g. see

[1]), significantly less cyclic cohesive zone models have been developed, e.g. [2, 3, 4, 5, 6, 7]. In contrast to the evaluation of the PARIS equation, cycle-by-cycle FE analyses with cyclic cohesive zone models also cover complex cyclic loading sequences. Of course, limitations arise from computational costs and often the identification of the model parameters is an open question. Although the correlation between the model parameters and the PARIS parameters is examined in e.g. [4, 7], there is still a lack of information in which way the threshold value of a fatigue crack growth rate curve depends on the cohesive parameters. The present study tries to contribute to solution approaches concerning these problems. The main idea is to correlate the parameters of the cyclic cohesive zone model to experimental fatigue crack growth rate curves. Therefore, as it will be explained in Sec. 3, mode I fatigue crack growth of a semi-infinite crack under plane strain and small scale yielding conditions is considered. The corresponding boundary layer model is presented in Sec. 4. There and in the subsequent section where the definition of the crack extension is explained more in detail, the primary focus is the reliability of the results and the reduction of computational costs. Finally, the fatigue crack growth rate curve generated with the presented procedure is discussed.

In the following section, the cyclic cohesive zone model used is summarised (see also [8]).

2 CYCLIC COHESIVE ZONE MODEL

The constitutive behaviour of cohesive zones is described by the traction-separation law. In particular, it specifies the amount of traction transferred across the cohesive zone in dependence of the current displacement jump also known as separation and the damage state. For convenience, effective normalised quantities are introduced

$$\text{effective traction} \qquad \tau = \sqrt{t_\mathrm{n}^2 + t_\mathrm{r}^2 + t_\mathrm{s}^2}/t_0 \tag{1}$$

$$\text{effective separation} \qquad \lambda = \sqrt{\langle\delta_\mathrm{n}\rangle^2 + \delta_\mathrm{r}^2 + \delta_\mathrm{s}^2}/\delta_0 \tag{2}$$

with the material parameters cohesive strength t_0 and the corresponding separation δ_0. The indices $\mathrm{n}, \mathrm{r}, \mathrm{s}$ denote normal and tangential coordinates of the traction vector t_i and separation vector δ_i, respectively. The MacAulay brackets, $\langle\,\rangle$, indicate zero contribution of normal separation in compression case.

The present cyclic cohesive zone model captures monotonic as well as cyclic behaviour. Regarding the monotonic traction-separation relation, the exponential approach of Xu and Needleman [9] is used

$$\tau_\mathrm{mon} = \lambda \exp\left(1 - \lambda\right) \quad . \tag{3}$$

Figure 1 shows the respective traction-separation curve in normalised form. The area under the curve specifies the normalised fracture energy density $\Gamma_0 = \mathrm{e}$ with $G_0 = t_0\delta_0\Gamma_0$ being the fracture energy density and EULER's number e. If the magnitude of the traction vector equals the cohesive strength, damage initiates. The softening branch right of the

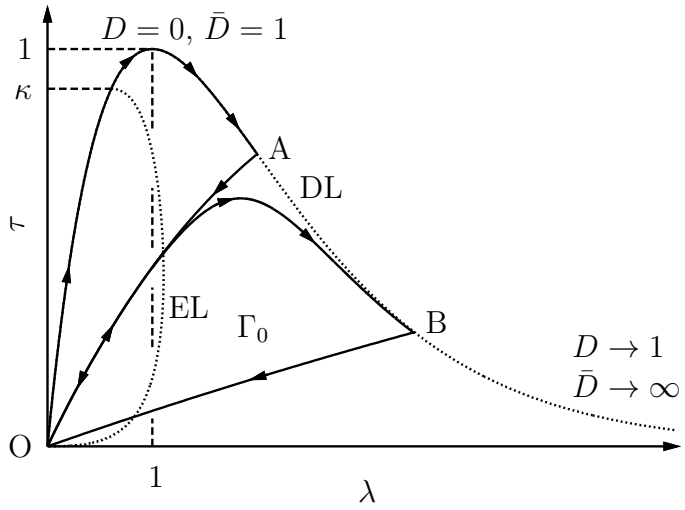

Figure 1: Cyclic cohesive zone model: dotted – exponential damage locus (DL), endurance locus (EL); solid – example of cyclic separation (path O – A – O – B – O)

apex is called damage locus. Here the damage evolves with increasing separation until no traction is transferred any longer indicating complete material failure. A separation-type fundamental scalar damage variable, $1 \leq \bar{D} \leq \infty$, is proposed to characterise the damage state. A conversion to the damage variable commonly used in damage mechanics, $0 \leq D \leq 1$, is performed by

$$D = \left[1 - \exp\left(\frac{1-\bar{D}}{\beta}\right)\right]^{\gamma} \quad , \tag{4}$$

introducing two further parameters β and γ. Note that this conversion is pure post-processing for visualisation purpose. It does not affect the damage state. Prior to damage initiation, reversible behaviour with unique un- and reloading paths at the traction-separation curve is assumed. Once damage is initiated these paths change according to an unloading function $F(\bar{D})$, see Fig. 2. This description guarantees a smooth transition from reversible to damaged state without any spurious dissipation. With

$$F = \begin{cases} -\frac{1}{\bar{D}}\,\mathrm{W}\left(-\bar{D}\exp(-\bar{D})\right) & ,\ \forall \bar{D} \geq 1 \\ 1 & ,\ \forall \bar{D} < 1 \end{cases} \quad . \tag{5}$$

and

$$t_i = \frac{\partial \Gamma}{\partial \delta_i} \quad , \quad i = \mathrm{n}, \mathrm{r}, \mathrm{s} \tag{6}$$

the cohesive potential Γ

$$\Gamma = \frac{t_0 \delta_0 \mathrm{e}}{F}\left[1 - [1 + \lambda F]\exp(-\lambda F)\right] \tag{7}$$

is formulated wherein the LAMBERT function $\mathrm{W}(x)$ (also known as product logarithm) is defined implicitly by

$$x = \mathrm{W}(x)\exp(\mathrm{W}(x)) \quad . \tag{8}$$

The description of the non-linear damage dependent unloading path follows from (7), (6) and (1)

$$\tau = \lambda F \exp(1 - \lambda F) \tag{9}$$

as also depicted in Fig. 1.

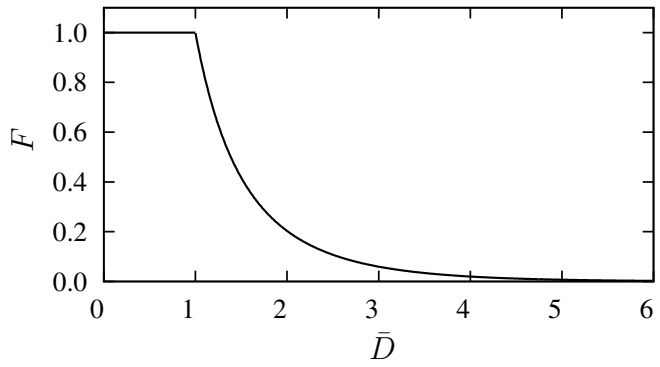

Figure 2: Unloading function, F, in dependence of the fundamental damage variable, $\bar{D}$

Under cyclic loading conditions un- and reloading paths differ beyond a damage dependent endurance limit expressed in terms of separation or traction using (9)

$$\text{endurance separation} \qquad \lambda_\mathrm{e} = -\frac{1}{F}\,\mathrm{W}\left(-\frac{\kappa}{\mathrm{e}}\left[\bar{D}\exp\left(1-\bar{D}\right)\right]^{\alpha}\right) \tag{10}$$

$$\text{endurance traction} \qquad \tau_\mathrm{e} = \lambda_\mathrm{e} F \exp(1 - \lambda_\mathrm{e} F) \quad . \tag{11}$$

Below the endurance limit un- and reloading paths coincide even for infinite cycling. Damage now initiates at the initial endurance traction κ, which lies on the ascending part of the normalised monotonic traction-separation curve, see Fig. 1. The τ_e-λ_e curve determined by the parameters κ and α is called endurance locus. Assuming $\alpha = 1$ and $\kappa = 1$, the cyclic cohesive zone model becomes monotonic. Beyond the endurance limit damage evolves according to the damage evolution equation

$$\dot{\bar{D}} = \left(\frac{\lambda}{\bar{D}}\right)^{r} \langle\dot{\lambda}\rangle\, \mathrm{H}(\lambda - \lambda_\mathrm{e}) \tag{12}$$

wherein the damage exponent r controls the damage rate. The endurance limit is incorporated by evaluating the HEAVISIDE function $\mathrm{H}(\,)$ in the rightmost term of (12). Figure 1

shows the traction-separation relation and the damage evolution during cyclic loading. Note that the endurance locus and the damage locus can be seen as lower and upper bounds for damage evolution, respectively.

The cyclic cohesive zone model comprises 5 free parameter: t_0, G_0, κ, α, r. With a fixed shape of the traction-separation curve, the intrinsic length is obtained by $\delta_0 = G_0/(t_0\Gamma_0) = G_0/(t_0\mathrm{e})$. Assuming D as the ratio between local dissipation density and fracture energy density, the remaining parameters are found as $\beta = 1.57$ and $\gamma = 1.69$.

In order to perform finite element analyses, the presented cyclic cohesive zone model was implemented as FORTRAN subroutine using the ABAQUS UEL interface. For detailed information concerning the finite element formulation see e.g. [10].

3 SEMI-INFINITE CRACK UNDER SMALL SCALE YIELDING

In order to investigate the influences of the cohesive zone model parameters on fatigue crack growth, a semi-infinite crack under plane strain and small scale yielding conditions is considered. According to the first term of the Williams series expansion, the far field is determined by the stress intensity factor K_I leading to mode I crack propagation. For convenience, the matrix material is assumed to be isotropic and linear elastic with Young's modulus E and Poisson ratio ν. Thus only the cohesive zone contributes to dissipation.

Cyclic load is applied in terms of load ratio, R, and maximum load, $K_\mathrm{I}^\mathrm{max}$. With respect to minimum load, $K_\mathrm{I}^\mathrm{min}$, and cyclic stress intensity factor, ΔK_I, the following applies

$$R = \frac{K_\mathrm{I}^\mathrm{min}}{K_\mathrm{I}^\mathrm{max}} \quad , \tag{13}$$

$$\Delta K_\mathrm{I} = K_\mathrm{I}^\mathrm{max} - K_\mathrm{I}^\mathrm{min} = K_\mathrm{I}^\mathrm{max}(1-R) \quad , \tag{14}$$

$$K_\mathrm{I}^\mathrm{min} = RK_\mathrm{I}^\mathrm{max} = \frac{R\Delta K_\mathrm{I}}{1-R} \quad . \tag{15}$$

Linear elastic fracture mechanics allows the conversion of K_I to the energy release rate, G,

$$G = \frac{1-\nu^2}{E} K_\mathrm{I}^2 \quad , \tag{16}$$

$$\Delta G = \frac{1-\nu^2}{E} \left(K_\mathrm{I}^\mathrm{max}\right)^2 \left(1-R^2\right) \quad . \tag{17}$$

With regard to the cyclic cohesive zone model presented above, upper and lower bounds of $K_\mathrm{I}^\mathrm{max}$ are derived. The load leading to static failure, K_0, refers to the fracture energy density and forms the upper bound in normalised form

$$\frac{K_0}{t_0\sqrt{\delta_0}} = \sqrt{\left(\frac{E}{t_0}\right)\frac{\Gamma_0}{1-\nu^2}} \ , \quad \text{with } \Gamma_0 = \mathrm{e} \quad . \tag{18}$$

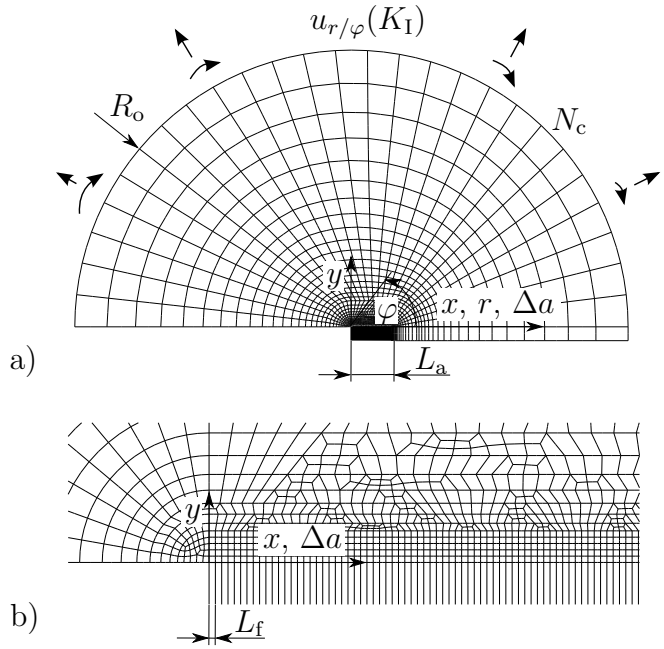

Figure 3: a) Boundary layer model with K_I-controlled displacement boundary conditions; b) detailed mesh within the fine meshed region, $0 \leq x \leq L_\mathrm{a}$

In contrast, damage initiation under cyclic loading conditions depends on the initial endurance limit, κ. This leads to the lower bound

$$\frac{K_\mathrm{i}}{t_0\sqrt{\delta_0}} = \sqrt{\left(\frac{E}{t_0}\right)\frac{\Gamma_\mathrm{i}}{1-\nu^2}}\ , \quad \text{with } \Gamma_\mathrm{i} = \mathrm{e} - \kappa + \frac{\kappa}{\mathrm{W}(-\frac{\kappa}{\mathrm{e}})}\ . \tag{19}$$

Fatigue crack growth analyses were performed applying loads in the ranges $0 \leq R \leq 0.8$ and $K_\mathrm{i}(\kappa) \leq K_\mathrm{I}^\mathrm{max} \leq K_0$. The respective finite element model is presented in the following.

4 BOUNDARY LAYER MODEL

In this section the finite element modelling of the boundary layer is addressed. Here, only a half of the model is meshed with finite elements for reasons of symmetry. The cohesive zone is located in the ligament to cover straight crack propagation. Figure 3 a) shows a sketch with the most important modelling parameters. The height of the cohesive zone is displayed just for visualisation purpose. The only geometric quantitiy is the outer radius R_o. At the outer rim, K_I controlled displacement boundary conditions are applied according to the far field solution. This implies that the crack tip is always presumed to be at the center of the model. Thus, R_o must be much larger than the expected crack length extension, Δa. Parameter variations reveal, that $R_\mathrm{o} = 10^8\delta_0$ allows crack growth up to $\Delta a = 10^3\delta_0$ assuming constant loading conditions.

The number of finite elements at the outer rim is chosen as $N_\mathrm{c} = 20 - 30$. Both quantities, R_o and N_c, have minor influences on the finite element models number of nodes

and thus overall computational costs. In contrast, the fine cohesive element length, L_f, and the width of the maximum expected crack extension, i.e. the fine meshed region, L_a, are of remarkable significance (see Fig. 3). In order to save computational costs, several models differing in L_f and L_a were generated. Since mesh refinement over orders of magnitudes with standard ABAQUS CAE meshing tools leads to exceeding numbers of nodes, an iterative partitioning and meshing algorithm using the ABAQUS CAE biased seeding techniques was developed. Figure 4 exemplarily shows the resulting linear relationship between the models number of nodes and L_a with $L_\mathrm{f} = 0.01\delta_0$ kept constant. The latter was found by convergence studies. In order to limit the model size, a larger value is chosen for higher load levels.

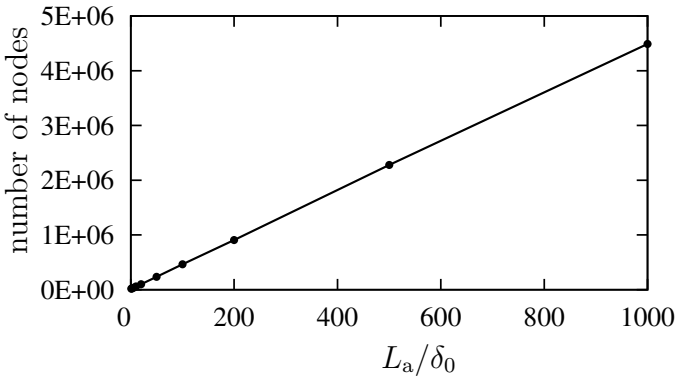

Figure 4: Number of nodes of finite element boundary layer models in dependence of the width of the fine meshed region $L_\mathrm{a} = \{10, 20, 50, 100, 200, 500, 1000\}\delta_0$ with $L_\mathrm{f} = 0.01\delta_0$

5 FATIGUE CRACK GROWTH

In this section the generation of fatigue crack growth rate curves ($\frac{\mathrm{d}\,a}{\mathrm{d}\,N}$ vs. $\frac{\Delta K_\mathrm{I}}{K_0}$) with the help of the FE boundary layer model is demonstrated.

5.1 Modelling Aspects

Fatigue crack growth rate curves typically consist of a near-threshold stage, the Paris region of fatigue crack growth implying a power-law relationship, and static failure. With about 30 simulations in the load range described above (with R kept constant) these ranges are covered. Simulations with lower load levels were performed with $L_\mathrm{f} = 0.01\delta_0$ and $L_\mathrm{a} = 100\delta_0$, higher load levels with $L_\mathrm{f} = 0.05\delta_0$ and $L_\mathrm{a} = 1000\delta_0$, respectively.

Due to the large number of simulations, a further reduction of computational costs is of special interest. Besides the model size, the most important parameters concerning computational cost are of course the number of load cycles and the time incrementation. In order to record fatigue crack growth rate curves, an individual simulation can be aborted once the crack growth rate has stabilized and a certain number of cycles at this steady state has been performed. For this purpose, online supervising was established using

the ABAQUS URDFIL interface. As a global measure, the magnitude of the oscillating dissipated energy of the whole model is evaluated, which, as stated above, only comes from the cohesive zone. After 30 cycles with constant dissipation magnitude the URDFIL aborts the simulation. The URDFIL was also used to control the time incrementation. The complete reversible unloading stages due to the load ratio $R \geq 0$ allow an elevated time increment decreasing the computational costs significantly. Convergence studies were performed to find appropriate increments. The crack extension was evaluated as depicted in Fig. 5 leading to 10 and 5 increments for loading and unloading, respectively.

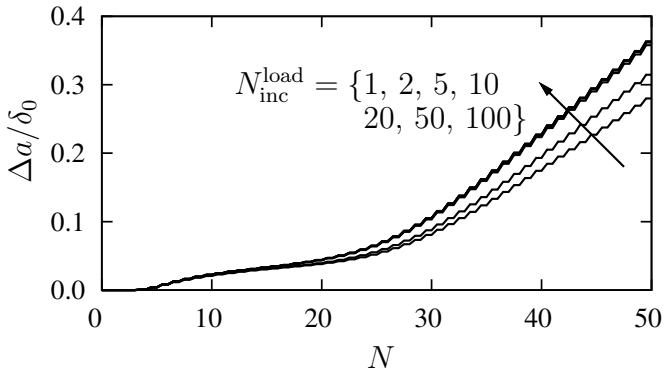

Figure 5: Crack extension vs. number of load cycles for increasing number of time increments in the loading case

There are two possibilities to measure the crack extension, Δa. The first damage based method evaluates the damage distribution at the ligament

$$\Delta a = \int_{\text{CZ}} D(x)\,\mathrm{d}\,x \quad . \tag{20}$$

interpreting the damage variable as an effective surface density of microdefects [11]. Since D depends on the fundamental damage by (4), the fitting parameters β and γ have an influence on the resulting crack length. This is the major drawback of this method because (4) applies only under monotonic loading conditions. Nevertheless, once the development of the damage zone is completed, the amount of crack growth does not depend on β and γ any longer which suffices for our purposes. Damage zones, i.e. the distributions of damage at the ligament after different numbers of load cycles, are depicted in Fig. 6 a). Fully developed damage zones exhibit a damage range of $0 \leq D \leq 1$ and a constant width. With ongoing cycling the crack grows by constant increments $\Delta\Delta a$ with each cycle. The second method assumes the location of the maximum stress in the cohesive zone to be the current crack tip position

$$\Delta a = x(\tau_{\max}) \quad . \tag{21}$$

This stress based crack length measure again only applies for a fully developed damage zone. Under this condition the results of both methods coincide. Respective traction profiles are plotted in Fig. 6 b).

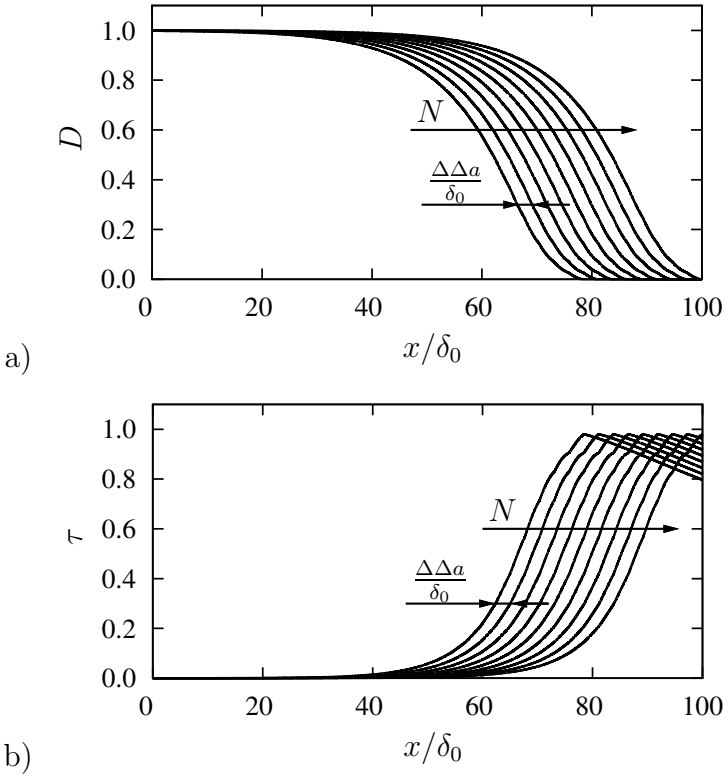

Figure 6: Profiles at the ligament with increasing number of cycles, N, and constant crack growth increment $\Delta\Delta a$: a) damage distributions and b) respective effective traction distributions

Furthermore, to ensure the validity of (20), the URDFIL also aborts the fatigue crack growth analyses whenever the damage zone exceeds L_a, see Fig. 7.

5.2 Results

Figure 7 shows fatigue crack growth curves generated with the algorithm presented above. As shown there, at least for higher loads the stabilised fatigue crack growth rate increases with increasing load level. Each fatigue crack growth curve provides one point to the fatigue crack growth rate curve depicted in Fig. 8. In this particular case 28 simulations were performed with a parameter set of $\kappa = 0.9$, $\alpha = 5$, $r = 1$, $E = 100t_0$, $\nu = 0.3$ and $R = 0$ which also refers to Fig. 6.

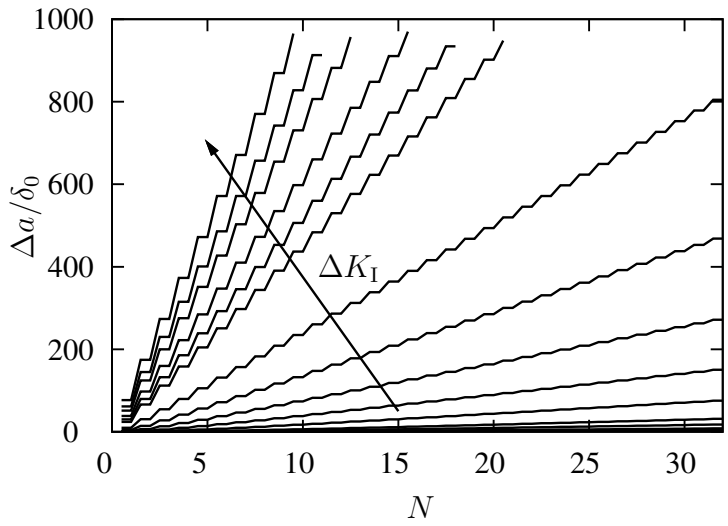

Figure 7: Fatigue crack extension, $\Delta a/\delta_0$, in dependence of the number of load cycles, N, for increasing load ranges, ΔK_I; for high load levels $\Delta a > L_\mathrm{a} = 1000\delta_0$ triggers the analysis abortion controlled by URDFIL

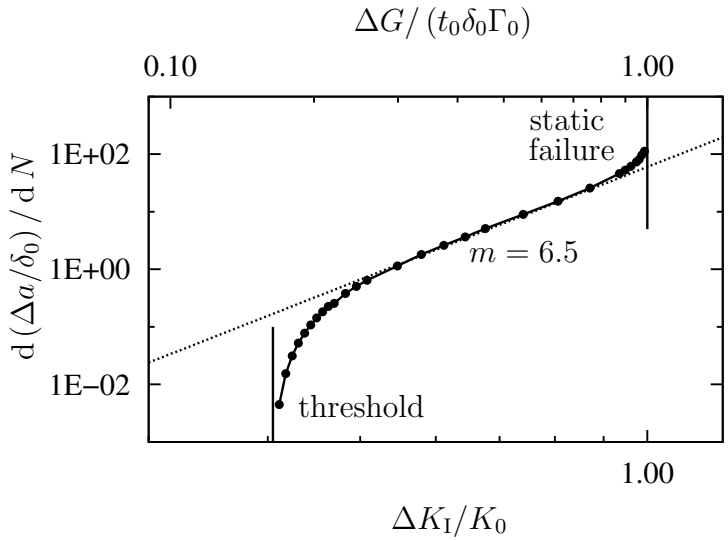

Figure 8: Normalised fatigue crack growth rate, $\mathrm{d}(\Delta a/\delta_0)/\mathrm{d}\,N$, in dependence of normalised applied load range, $\Delta K_\mathrm{I}/K_0$, and $\Delta G/(t_0\delta_0\Gamma_0)$, respectively ($R = 0$); dotted: straight line of PARIS law with exponent $m = 6.5$

As expected, the fatigue crack growth rate curve comprises the three regions of fatigue crack growth. The threshold value is found as $\Delta K_\mathrm{th} \approx 0.41K_0$, static failure occurs at $\Delta K_\mathrm{I} = K_0$. The PARIS exponent which is the slope of the linear region in the log-log plot gives $m = 6.5$. It should emphasised that these values do not correlate to a specific

material since the parameters of the cohesive law are chosen arbitrarily. But nevertheless the results of this study show that the modelling procedure presented is suitable for further studies on the fatigue crack growth behaviour employing the cyclic cohesive zone approach.

6 SUMMARY AND CONCLUSIONS

In this paper the modelling of fatigue crack growth using a cohesive zone approach is presented. In order to develop a parameter identification algorithm, the influences of the constituents used in the cyclic cohesive zone models on fatigue crack growth rate curves is of special interest. In the presented cyclic cohesive zone model this concerns the parameters defining the endurance locus, the damage exponent in the damage evolution equation and the fracture or cohesive energy, respectively. A FE model under plane strain and small scale yielding conditions is outlined. Thereby, the focus is on reducing computational costs. In particular, this relates to an appropriate load range, the choice of meshing and time incrementation parameters, and the abortion of the simulation once the fatigue crack growth has stabilised. Here, we make use of the ABAQUS URDFIL interface. The study shows exemplarily how a fatigue crack growth rate curve is generated. This places proper conditions for further parameter studies published elsewhere. The modelling procedure is not restricted to a specific cohesive model. Therefore, extensions to the cyclic cohesive zone model presented here can be considered, as well as the application to cohesive models from literature is worth investigating. Furthermore, overload and sequence effects should be analysed. Finally, in order to evoke crack closure effects, it is intended to include plasticity.

ACKNOWLEDGEMENT

This work was performed within the Cluster of Excellence “Structure Design of Novel High-Performance Materials via Atomic Design and Defect Engineering (ADDE)” that is financially supported by the European Union (European regional development fund) and by the Ministry of Science and Art of Saxony (SMWK).

REFERENCES

[1] Schwalbe, K.H., Scheider, I. and Cornec, A. *Guidelines for Applying Cohesive Models to the Damage Behaviour of Engineering Materials and Structures*. Springer (2013).

[2] Nguyen, O., Repetto, E., Ortiz, M. and Radovitzky, R. A cohesive model of fatigue crack growth. *International Journal of Fracture* (2001) **110**(4):351–369.

[3] Yang, B., Mall, S. and Ravi-Chandar, K. A cohesive zone model for fatigue crack growth in quasibrittle materials. *International Journal of Solids and Structures* (2001) **38**(22-23):3927–3944.

[4] Roe, K. and Siegmund, T. An irreversible cohesive zone model for interface fatigue crack growth simulation. *Engineering Fracture Mechanics* (2003) **70**(2):209–232.

[5] Lucas, L., Black, T. and Jones, D. Use of cohesive elements in fatigue analysis. In: *American Society of Mechanical Engineers, Pressure Vessels and Piping Division (Publication) PVP*, vol. 2. ASME (2008) 13–25.

[6] Bouvard, J., Chaboche, J., Feyel, F. and Gallerneau, F. A cohesive zone model for fatigue and creep-fatigue crack growth in single crystal superalloys. *International Journal of Fatigue* (2009) **31**(5):868–879.

[7] Xu, Y. and Yuan, H. On damage accumulations in the cyclic cohesive zone model for xfem analysis of mixed-mode fatigue crack growth. *Computational Materials Science* (2009) **46**(3):579–585.

[8] Roth, S. and Kuna, M. Numerical study on interfacial damage of sprayed coatings due to thermo-mechanical fatigue. In: E. Onate, D. Owen, D. Peric and B. Suarez, eds., *XI International Conference on Computational Plasticity. Fundamentals and Applications. COMPLAS XI.* (2011) .

[9] Xu, X.P. and Needleman, A. Void nucleation by inclusion debonding in a crystal matrix. *Modelling and Simulation in Materials Science and Engineering* (1993) **1**(2):111–132.

[10] Ortiz, M. and Pandolfi, A. Finite-deformation irreversible cohesive elements for three-dimensional crack-propagation analysis. *International Journal for Numerical Methods in Engineering* (1999) **44**(9):1267–1282.

[11] Lemaitre, J. *A course on damage mechanics*. Springer, 2nd edn. (1996).